Cold Nuclear Matter Effects on J/ψ Production at High Baryon Densities

R. Vogt

Lawrence Livermore National Laboratory, Livermore, CA 94551, USA
Physics and Astronomy Department, UC Davis, Davis, CA 95616, USA

based on:
RV, arXiv:2101.02858, Phys. Rev. C 103, 035204 (2021)

Figure 1: This work was performed under the auspices of the U.S. Department of Energy by Lawrence Livermore National Laboratory under Contract DE-AC52-07NA27344 and the LLNL-LDRD Program under Project No. 21-LW-034.

Intrinsic Charm is Long-standing Puzzle in QCD

An intrinsic charm component of the hadron wavefunction, $|uudc\bar{c}\rangle$, was first proposed by Brodsky, Hoyer, Peterson and Sakai in the 1980's

If this state is the dominant Fock component, its invariant mass is minimized, giving the charm quarks a larger fraction of the hadron momentum and leading to enhanced charm production in the forward region

A number of experimental hints have been seen, no conclusive results

- **EMC charm structure function, F_2^c, large at largest x and highest Q^2 measured in experiment**
- **Leading charm asymmetries (D^- over D^+ in $\pi^- p$ interactions, E791) consistent with intrinsic charm predictions**
- **Double J/ψ production observed at high pair x_F by NA3**
- **Forward charm production observed in many fixed-target experiments (WA82, WA89, E791, SELEX and others)**
- **Proposed explanation of high energy astrophysical neutrino rate at Ice Cube (Brodsky and Laha)**

At colliders, forward x_F pushed to very high rapidity and detection is less likely, at least for J/ψ production, lower energy, fixed-target configurations may be better for discovery measurement

LHCb: Evidence of Intrinsic Charm in $Z + c$-Jet Events

$Z+c$-jet ratio to Z+all-jet events at $\sqrt{s} = 13$ TeV is more consistent with calculations including intrinsic charm at high $y(Z)$, up to 1% intrinsic charm content

Differences between calculations without intrinsic charm (no IC) and intrinsic charm allowed calculations, either with NNPDF 3.0 including IC or CT14 with a 1% IC content, grows larger with increasing $y(Z)$

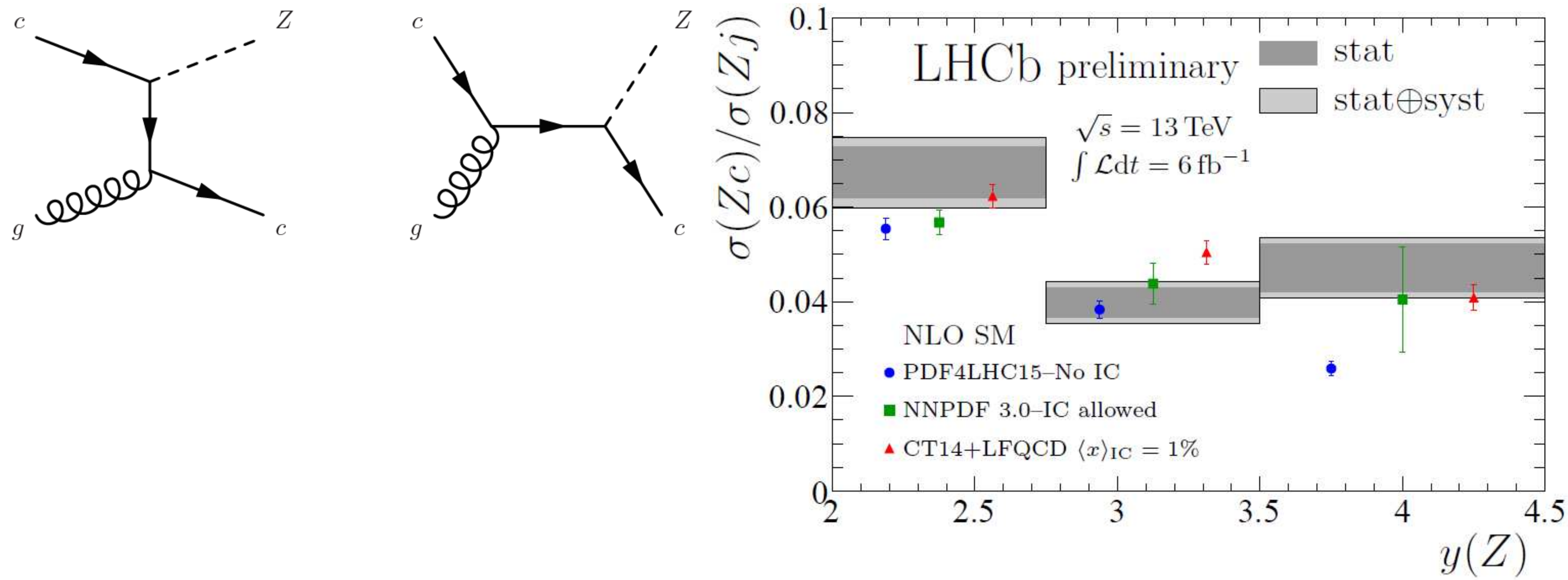

Figure 2: (Left) Leading order diagrams producing $Z + c$-jet events. (Right) Ratio of $Z + c$-jets to Z+all-jet events from LHCb. Images from https://lhcb-public.web.cern.ch/Welcome.html#IC, 27 July 2021.

NA60+ May Be Useful for Intrinsic Charm Searches

In low energy, fixed-target setups, intrinsic charm is more likely to be present near midrapidity

Recently, the SeaQuest experimental used a 120 GeV proton beam on proton and nuclear targets: p+p, p+d, p+C, p+Fe **and** p+W **at high** x_F **and low** p_T, $0.4 < x_F < 0.95$ **and** $p_T < 2.3$ **GeV (data not yet public)**

Results can be tested against calculations for the E866/NuSea experiment also at FNAL but at higher energy: they used

E866 covered full forward x_F **range with an 800 GeV proton beam on proton, Be, Fe and W targets. They covered** $-0.1 < x_F < 0.95$ **and looked at the** p_T **dependence in 3 different** x_F **bins: low** x_F **(**$-0.1 \leq x_F \leq 0.3$**); intermediate** x_F **(**$0.2 \leq x_F \leq 0.6$**); high** x_F **(**$0.3 \leq x_F \leq 0.95$**)**

NA60+ will go to lower energies than SeaQuest with proton beams at 40, 80, and 120 GeV, studied $p + \mathrm{Pb}$ **interactions relative to** $p + p$ **here, calculations are as a function of** p_T **over all rapidity and as a function of** y **over all** p_T

Components of Model Calculation

Nuclear suppression factor includes both perturbative cross section and production by intrinsic charm:

$$\begin{aligned} \sigma_{pA} &= \sigma_{\rm CEM}(pA) + \sigma_{\rm ic}^{J/\psi}(pA) \\ \sigma_{p{\rm d}} &= 2\sigma_{\rm CEM}(pp) + \sigma_{\rm ic}^{J/\psi}(pA) \end{aligned}$$

$\sigma_{\rm CEM}$ **is the production cross section computed at NLO in the color evaporation model for** $p+p$ **and** $p+A$ **interactions**

$\sigma_{\rm ic}^{J/\psi}$ **is intrinsic charm production cross section including the probability for an intrinsic charm contribution to the proton wavefunction**

Components of all terms are discussed in detail in the following slides

Charmonium Production in Color Evaporation Model

The CEM at NLO is employed for the perturbative production cross section:

$$\sigma_{\rm CEM}(pp) = F_C \sum_{i,j} \int_{4m^2}^{4m_H^2} ds \int dx_1 \, dx_2 \; F_i^p(x_1, \mu_F^2, k_{T_1}) \; F_j^p(x_2, \mu_F^2, k_{T_2}) \; \hat{\sigma}_{ij}(\hat{s}, \mu_F^2, \mu_R^2)$$

Parton densities factorized into longitudinal (CT10) and a k_T-dependent component to implement k_T broadening a la low p_T resummation

$$F^p(x, \mu_F^2, k_T) = f^p(x, \mu_F^2) G_p(k_T)$$

$$\begin{aligned} g_p(k_T) &= G_p(k_{T_1}) G_p(k_{T_2}) \\ g_p(k_T) &= \frac{1}{\pi \langle k_T^2 \rangle_p} \exp(-k_T^2 / \langle k_T^2 \rangle_p) \end{aligned}$$

$$\langle k_T^2 \rangle_p = \left[1 + \frac{1}{n} \ln \left(\frac{\sqrt{s_{NN}}(\mathrm{GeV})}{20\,\mathrm{GeV}} \right) \right] \; \mathrm{GeV}^2$$

$\langle k_T^2 \rangle_p$ broadening assumed energy dependent, $n = 12$ from J/ψ data; at $p_{\rm lab} = 40$, 80 and 120 GeV, $\sqrt{s_{NN}} = 8.77$, 12.33 and 15.4 GeV respectively, $\langle k_T^2 \rangle_p = 0.72$, 0.84 and 0.97 GeV^2 Uncertainty band on cross section set by:

$$\begin{aligned} \frac{d\sigma_{\rm max}}{dX} &= \frac{d\sigma_{\rm cent}}{dX} + \sqrt{\left(\frac{d\sigma_{\mu,{\rm max}}}{dX} - \frac{d\sigma_{\rm cent}}{dX} \right)^2 + \left(\frac{d\sigma_{m,{\rm max}}}{dX} - \frac{d\sigma_{\rm cent}}{dX} \right)^2} \\ \frac{d\sigma_{\rm min}}{dX} &= \frac{d\sigma_{\rm cent}}{dX} - \sqrt{\left(\frac{d\sigma_{\mu,{\rm min}}}{dX} - \frac{d\sigma_{\rm cent}}{dX} \right)^2 + \left(\frac{d\sigma_{m,{\rm min}}}{dX} - \frac{d\sigma_{\rm cent}}{dX} \right)^2} \end{aligned}$$

J/ψ Distributions in CEM at $\sqrt{s_{NN}} = 15.4$ GeV

Uncertainty bands defined by $(m, \mu_F/m_T, \mu_R/m_T) = (1.27 \pm 0.09\,\mathrm{GeV}, 2.1^{+2.55}_{-0.85}, 1.6^{+0.11}_{-0.12})$**;** μ_F**, factorization scale, and** μ_R**, renormalization scale, defined relative to pair transverse mass:** $\mu_{F,R} \propto m_T = \sqrt{m^2 + p_T^2}$ **where** $p_T^2 = 0.5(p_{T_Q}^2 + p_{T_{\overline{Q}}}^2)$

Scale uncertainties set by $\{(\mu_F/m_T, \mu_F/m_T)\} = \{(C,C)$**,** (H,H)**,** (L,L)**,** (C,L)**,** (L,C)**,** (C,H)**,** $(H,C)\}$ **(Mass uncertainties dominate.)**

Distributions become narrower for the lower energies

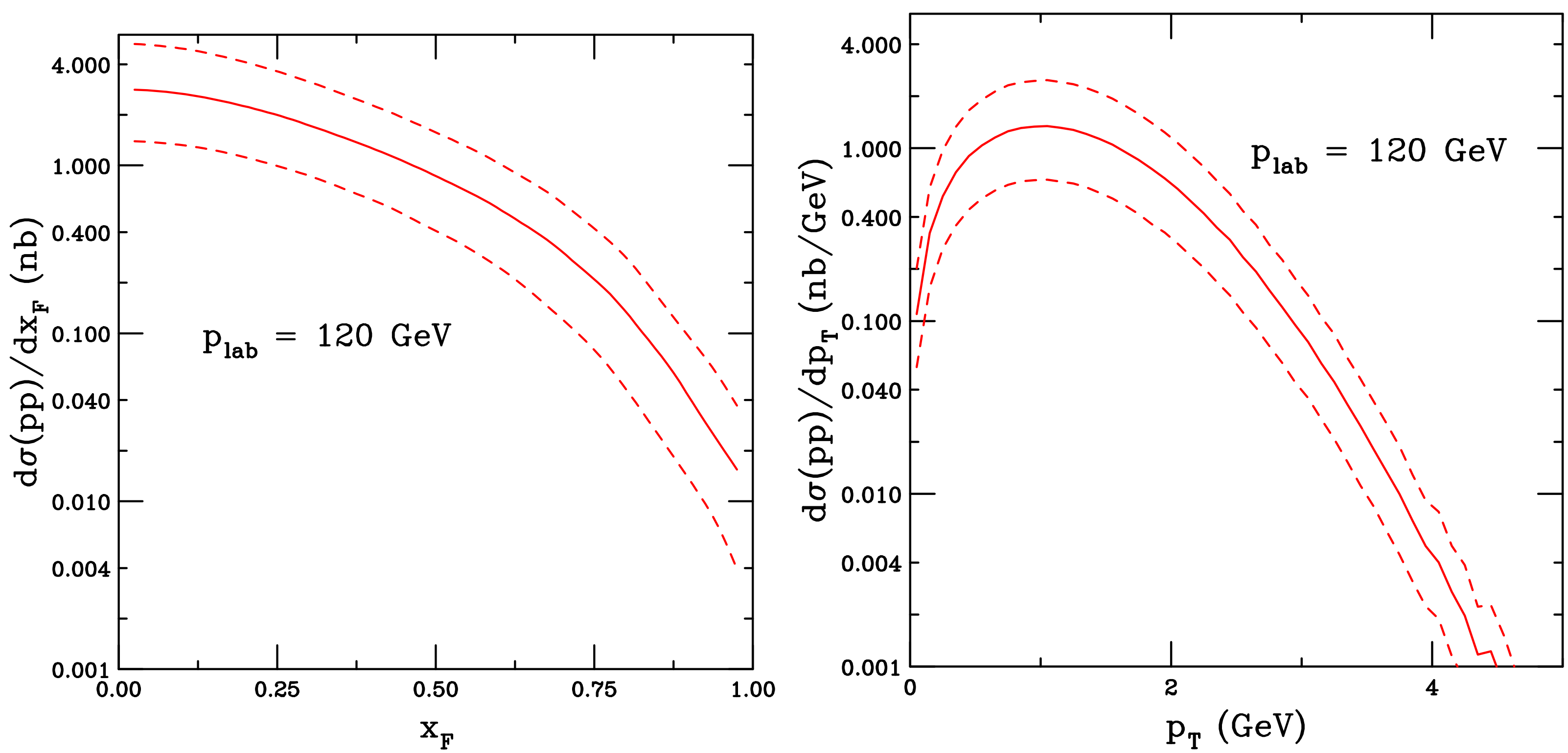

Figure 3: The J/ψ production cross sections in the CEM in $p+p$ collisions at $\sqrt{s} = 15.4$ GeV as a function of x_F (a) and p_T (b), integrated over all phase space, are shown. The solid curves show the central values while the dashed curves outline the upper and lower limits of the uncertainty band.

Cold Matter Effects on Perturbative Cross Section

Production cross section in a pA collision becomes

$$\sigma_{pA} = \sigma_{\rm CEM}(pA) = S_A^{\rm abs} F_C \sum_{i,j} \int_{4m^2}^{4m_H^2} ds \int dx_1 \, dx_2 \; F_i^p(x_1,\mu_F^2,k_T) \; F_j^A(x_2,\mu_F^2,k_T) \; \hat\sigma_{ij}(\hat s,\mu_F^2,\mu_R^2)$$

Survival probability for absorption of a (proto)charmonium state in nuclear matter

$$\begin{aligned}
\sigma_{pA} = \sigma_{pN} S_A^{\rm abs} &= \sigma_{pN} \int d^2b \int_{-\infty}^{\infty} dz \, \rho_A(b,z) S^{\rm abs}(b) \\
&= \sigma_{pN} \int d^2b \int_{-\infty}^{\infty} dz \, \rho_A(b,z) \exp\left\{ - \int_z^\infty dz' \rho_A(b,z') \sigma_{\rm abs}(z'-z) \right\}
\end{aligned}$$

Here the absorption cross section is assumed constant but note that prior experiments extracted an effective absorption cross section from A^α analysis with $\alpha = 1 - 9\sigma_{\rm abs}/(16\pi r_0^2)$ assuming no other nuclear effects

Nuclear parton densities

$$\begin{aligned}
F_j^A(x_2,\mu_F^2,k_T) &= R_j(x_2,\mu_F^2,A) f_j(x_2,\mu_F^2) G_A(k_T) \\
F_i^p(x_1,\mu_F^2,k_T) &= f_i(x_1,\mu_F^2) G_p(k_T)
\end{aligned}$$

For a deuteron target, $R_j \equiv 1$

$$g_A(k_T) = G_p(k_{T_1}) G_A(k_{T_2})$$

$G_A(k_T)$ **includes increased broadening in the nuclear target ($A > 2$)**

k_T Broadening in Nuclei

k_T **broadening in nuclei may arise from multiple scattering in the target, to implement broadening, a larger value of** $\langle k_T^2 \rangle$ **is used for nuclear targets**

$$\langle k_T^2 \rangle_A = \langle k_T^2 \rangle_p + \delta k_T^2$$

δk_T^2 **gives strength of broadening**

$$\delta k_T^2 = (\langle \nu \rangle - 1)\Delta^2(\mu)$$

The broadening strength depends on the interaction scale:

$$\Delta^2(\mu) = 0.225 \frac{\ln^2(\mu/\mathrm{GeV})}{1 + \ln(\mu/\mathrm{GeV})} \mathrm{GeV}^2 \qquad \mu = 2m_c$$

Strength also depends on number of scatterings proton undergoes passing through nuclear target, $\langle \nu \rangle - 1$

$$\langle \nu \rangle = \sigma_{pp}^{\mathrm{in}} \frac{\int d^2b T_A^2(b)}{\int d^2b T_A(b)} = \frac{3}{2} \rho_0 R_A \sigma_{pp}^{\mathrm{in}}$$

T_A **is the nuclear profile function, here** $\rho_0 = 0.16/\mathrm{fm}^3$, $R_A = 1.2A^{1/3}$, **and the inelastic** $p + p$ **cross section is** $\sigma_{pp}^{\mathrm{in}} \sim 30$ **mb for the energies considered here**

Assuming a Pb target, $\delta k_T^2 = 0.41$, **giving an average broadening in the nucleus of** $\langle k_T^2 \rangle_A = 1.12$, **1.25, and 1.38 GeV**^{2} **at** $p_{\mathrm{lab}} = 40$, **80 and 120 GeV, respectively**

At the E866 energy, $\sqrt{s_{NN}} = 38.8$ **GeV, giving** $\langle k_T^2 \rangle_p = 1.05$ **GeV**^{2} **and** $\langle k_T^2 \rangle_A = 1.15$, **1.3 and 1.44 GeV**^{2} **for Be, Fe, and W targets**

Nuclear Modification of the Parton Densities

EPPS16 nuclear parton density modifications differentiate between u and d valence quarks and all sea quarks; 20 parameters give 40 error sets + 1 central set

Uncertainties are determined by calculating cross section for each A with all error sets, adding differences around central set for each parameter in quadrature

Lower energies probe higher x, for $0 < y < 1$, the momentum fraction in the nucleus is in the antishadowing and EMC regions

$$f_j^A(x_2, \mu_F^2) = R_j(x_2, \mu_F^2, A) f_j^p(x_2, \mu_F^2)$$

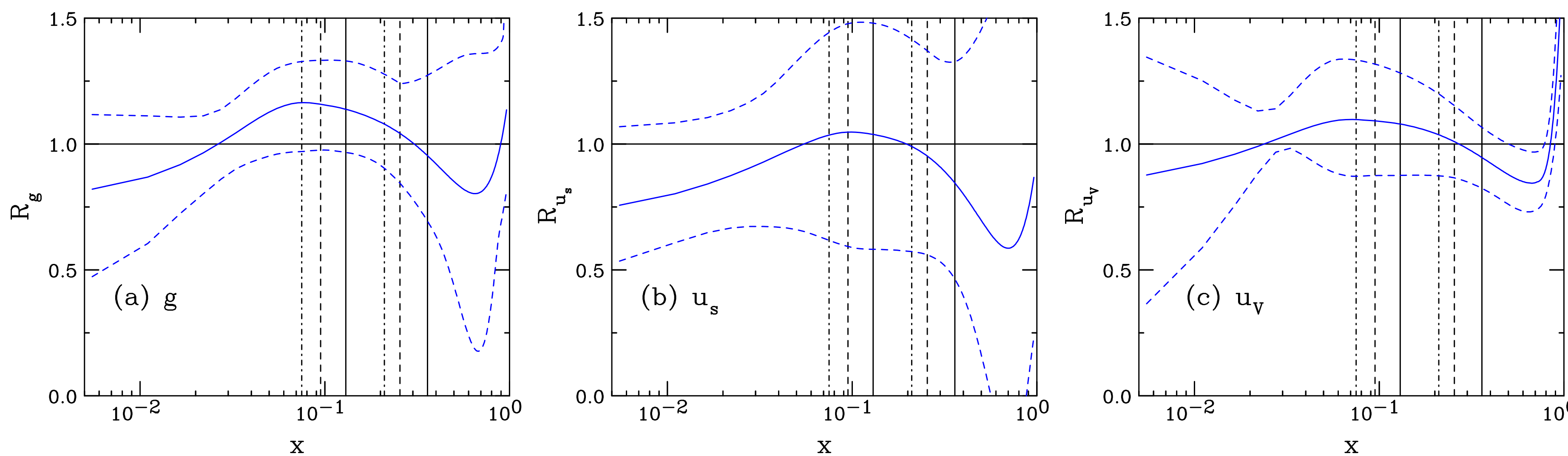

Figure 4: The EPPS16 ratios, with uncertainties, are shown at the scale of the J/ψ mass for gluons (a), the up sea quark distribution (b) and the valence up quark distribution (c) as a function of momentum fraction x. The central set is denoted by the solid curves while the dashed curves give the upper and lower limits of the uncertainty bands. The results are given for $A = 208$ (blue). The vertical lines indicate the x range relevant for $0 < y < 1$ for $p_{\rm lab} = 40$ (solid), 80 (dashed), and 120 (dot-dashed) GeV.

Interplay of Shadowing and Absorption

Depending on x values probed, shadowing can enhance or reduce absorption cross section needed to describe data

Absorption alone always gives less than linear A dependence ($\alpha < 1$)

For SPS energies, $17.3 \leq \sqrt{s_{NN}} \leq 29$ GeV, rapidity range covered is in EMC and antishadowing region, $\alpha > 1$ with no absorption

Adding shadowing to absorption in the SPS energy region requires a larger absorption cross section is needed to maintain agreement with data

For $\sqrt{s_{NN}} \geq 38$ GeV, x in shadowing regime, thus $\alpha < 1$ with shadowing alone in forward region, reducing needed absorption cross section to $\sigma_{\rm abs} \sim 0$ at the LHC

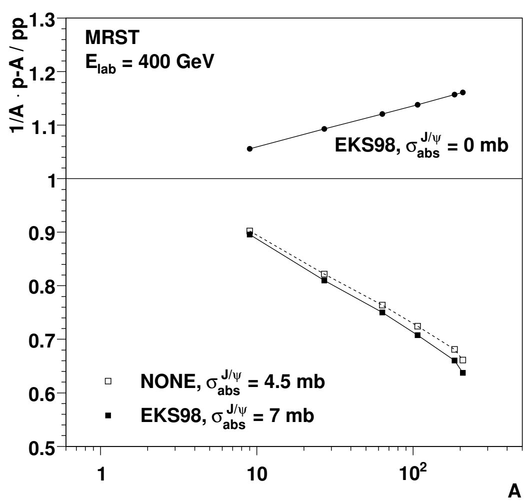

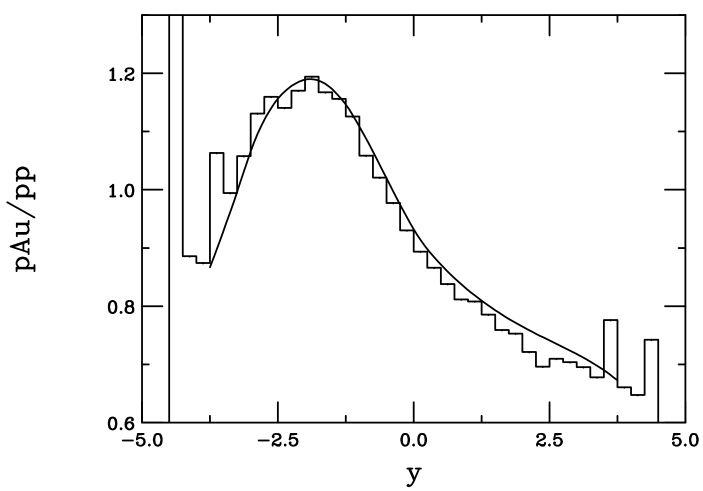

Figure 5: (Left) Illustration of the interplay between shadowing and absorption. [C. Lourenco, H. K. Woehri and RV, JHEP 0902 (2009) 014.] (Right) Comparison of LO and NLO shadowing ratios.

Energy Dependence of $\sigma_{\rm abs}^{J/\psi}$

At midrapidity, systematic decrease of $\sigma_{\rm abs}^{J/\psi}$ with $\sqrt{s_{NN}}$, independent of shadowing, trend continues at RHIC and above

$\sigma_{\rm abs}^{J/\psi}(y_{\rm cms} = 0)$ **at 158 GeV is significantly larger than that measured at 450 GeV**

Calculations confirmed by NA60 pA measurements at 158 GeV showing stronger absorption with L than at 400 GeV, suggesting $\sigma_{\rm abs}^{J/\psi} = 9$ mb at $\sqrt{s_{NN}} = 15.4$ GeV, 5 mb at $\sqrt{s_{NN}} = 38.8$ GeV, estimated $\sigma_{\rm abs}^{J/\psi} = 11$, 10 mb at $\sqrt{s_{NN}} = 12.3$, 8.8 GeV respectively

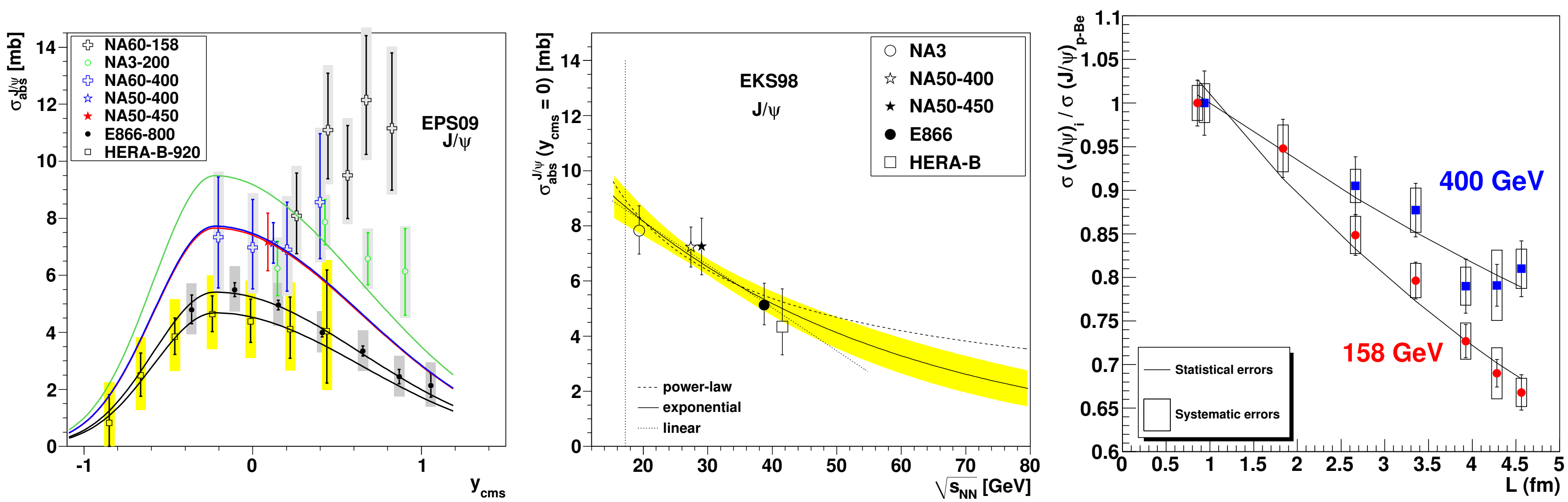

Figure 6: Left: Dependence of $\sigma_{\rm abs}^{J/\psi}$ on $y_{\rm cms}$ for all available data sets including EPS09 shadowing. The shape of the curves is fixed by the E866 and HERA-B data. [Lourenço, RV, Wöhri] Middle: The extracted energy dependence of $\sigma_{\rm abs}^{J/\psi}$ at midrapidity for power law (dashed), exponential (solid) and linear (dotted) approximations to $\sigma_{\rm abs}^{J/\psi}(y = 0, \sqrt{s_{NN}})$ using the EKS98 shadowing parameterization with the CTEQ61L parton densities. The band around the exponential curve indicates the uncertainty in the extracted cross sections at $x_F \sim 0$ from NA3, NA50 at 400 and 450 GeV, E866 and HERA-B. The vertical dotted line indicates the energy of the Pb+Pb and In+In collisions at the CERN SPS. [Lourenço, RV, Wöhri] Right: The J/ψ cross section ratios for pA collisions at 158 GeV (circles) and 400 GeV (squares), as a function of L, the mean thickness of nuclear matter traversed by the J/ψ.

Intrinsic Charm

Probability distribution of five-particle Fock state of the proton:

$$dP_{\mathrm{ic}\,5} = P^0_{\mathrm{ic}\,5} N_5 \int dx_1 \cdots dx_5 \int dk_{x\,1} \cdots dk_{x\,5} \int dk_{y\,1} \cdots dk_{y\,5} \frac{\delta(1 - \sum_{i=1}^5 x_i)\delta(\sum_{i=1}^5 k_{x\,i})\delta(\sum_{i=1}^5 k_{y\,i})}{(m_p^2 - \sum_{i=1}^5 (\widehat{m}_i^2/x_i))^2}$$

$i = 1, 2, 3$ **are** u, u, d **light quarks, 4 and 5 are** c **and** $\overline{c}$**,** N_t **normalizes the probability to unity and** P^0_{ic} **scales the normalized probability to the assumed intrinsic charm content: 0.1%, 0.31% and 1% are used to represent the range of probabilities assumed previously**

The IC cross section is determined from soft interaction scale breaking coherence of the Fock state, $\mu^2 = 0.1$ **GeV**^{2}

$$\sigma_{\mathrm{ic}}(pp) = P_{\mathrm{ic}\,5} \sigma^{\mathrm{in}}_{pN} \frac{\mu^2}{4\widehat{m}_c^2}$$

The J/ψ **cross section from intrinsic charm is then obtained by multiplying by the normalization factor for the CEM to the** J/ψ

$$\sigma^{J/\psi}_{\mathrm{ic}}(pp) = F_C \sigma_{\mathrm{ic}}(pp)$$

The A **dependence is**

$$\sigma^{J/\psi}_{\mathrm{ic}}(pA) = \sigma^{J/\psi}_{\mathrm{ic}}(pp)\, A^\beta$$

where $\beta = 0.71$ **for a proton beam on a nuclear target, as determined by NA3**

Intrinsic Charm x_F and p_T Distributions

Peak of the J/ψ x_F distribution is forward, at low energy, intrinsic charm is

p_T distribution is harder than the pQCD distribution at low energy; at higher energies and $x_F \sim 0$, the pQCD contribution will drown the intrinsic charm contribution

The p_T distribution also depends on range of k_T integrations, x_F distribution does not

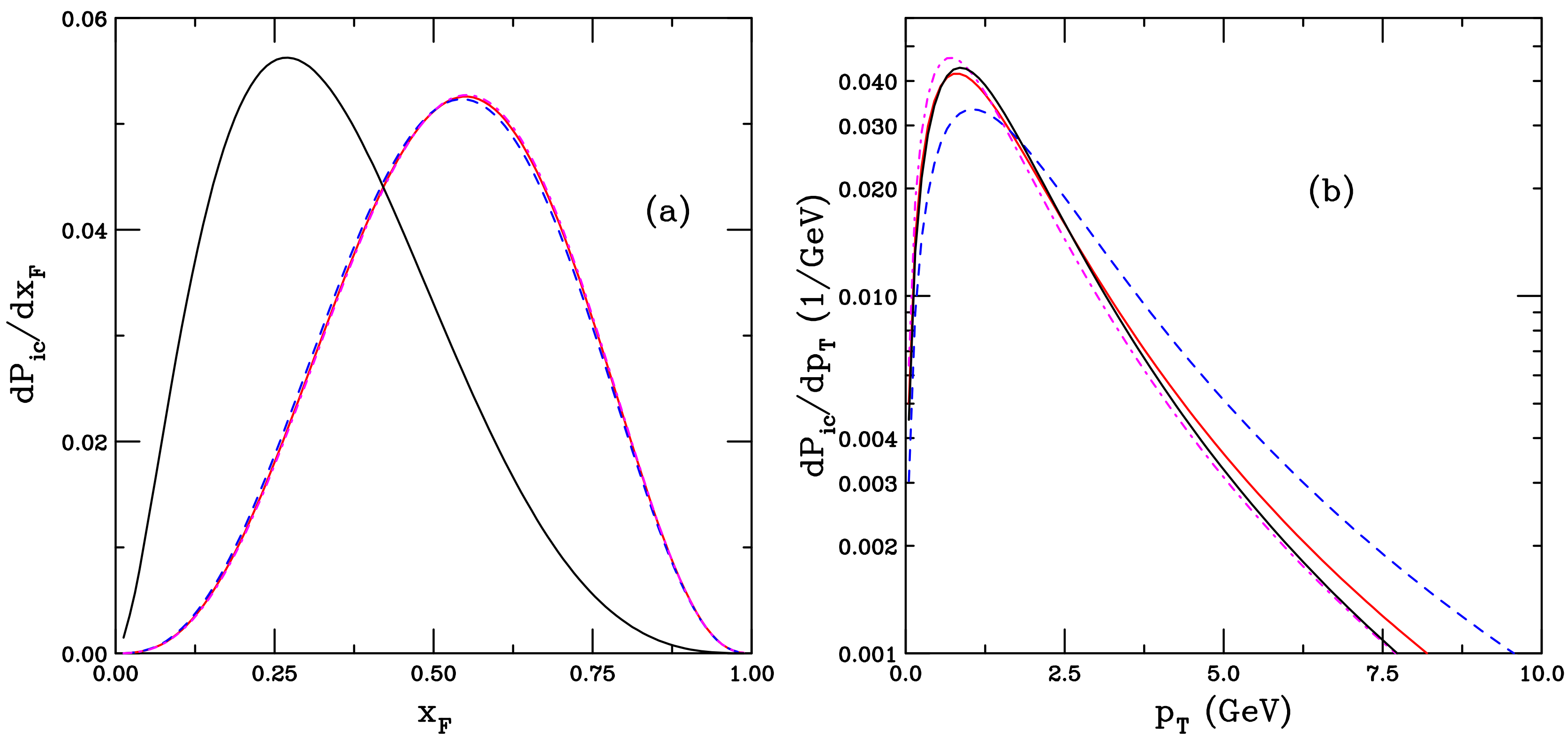

Figure 7: The probability distributions for J/ψ production from a five-particle proton Fock state as a function of x_F (a) and p_T (b). The results are shown for different values of the k_T range for the light and charm quarks. The red curve employs the default values, $k_q^{\max} = 0.2$ GeV and $k_c^{\max} = 1.0$ GeV while the blue dashed curve increases $k_q^{\max}$ and $k_c^{\max}$ by a factor of two and the dot-dashed magenta curve employs half the values of $k_q^{\max}$ and $k_c^{\max}$. The solid black curve shows the x and p_T distributions for a single charm quark from the state.

Intrinsic Charm y Distribution Depends on $\sqrt{s_{NN}}$

Once the x_F distribution is transformed to rapidity, it becomes sensitive to $\sqrt{s_{NN}}$ since $x_F = (2m_T/\sqrt{s_{NN}})\sinh y$

As $\sqrt{s_{NN}}$ increases, the intrinsic charm rapidity distribution is moved further away from midrapidity, taken to the extreme in the right-hand plot, showing the distribution also for $\sqrt{s_{NN}} = 7$ TeV, inaccessible to even most forward detectors

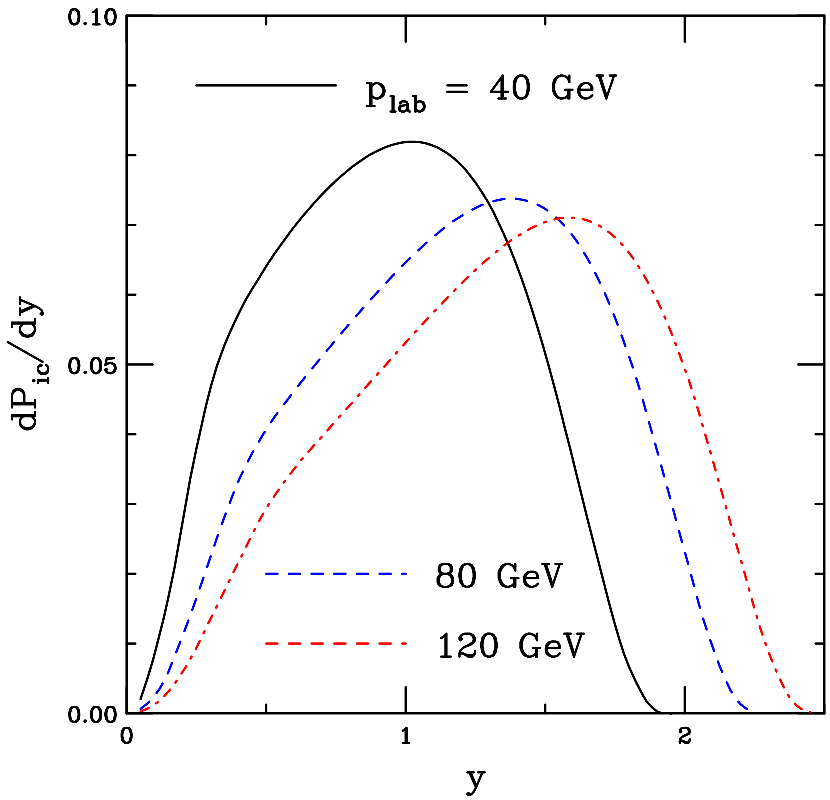

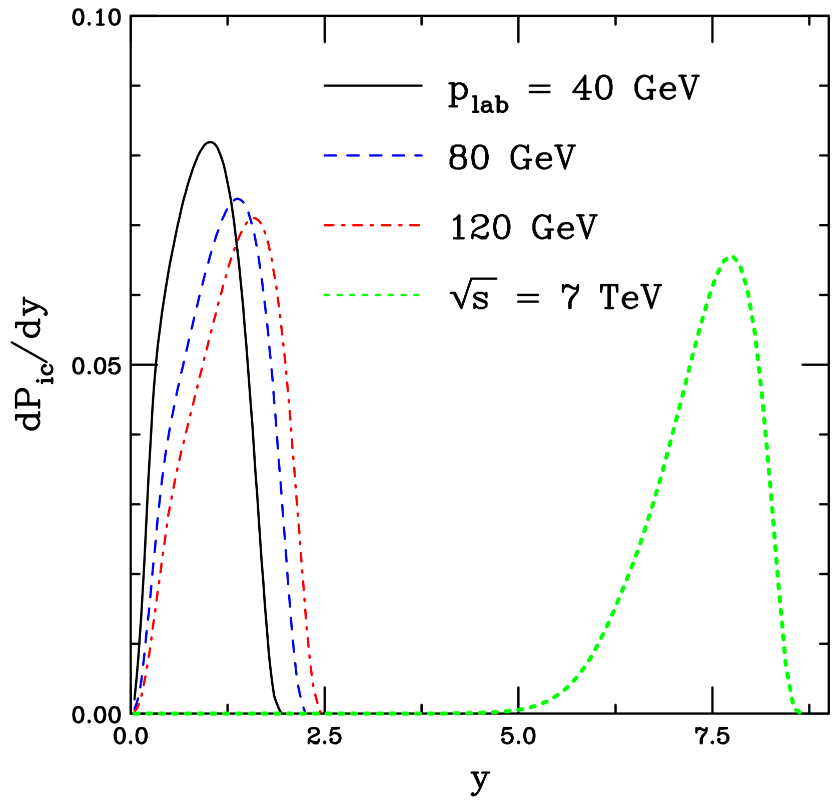

Figure 8: The probability distributions for J/ψ production from a five-particle proton Fock state as a function of y. The results are shown for different values of $\sqrt{s_{NN}}$. The solid black curve shows $\sqrt{s_{NN}} = 8.8$ GeV, the blue dashed curve is for $\sqrt{s_{NN}} = 12.3$ GeV, and the red dot-dashed curve is for $\sqrt{s_{NN}} = 15.4$ GeV. The results in (b) also include the green dotted curve for $\sqrt{s_{NN}} = 7$ TeV.

IC y Dependence on $k_T^{\max}$, m_i at $\sqrt{s_{NN}} = 15.4$ GeV

Left-hand plot shows the results of doubling and halving the k_T integration range; doubling the range shifts it backward, halving it moves it forward

Right-hand plot shows the results of increasing the charm quark mass from 1.27 GeV to 1.5 GeV and, with $m_c = 1.27$ GeV, reducing the light quark mass from 0.3 GeV to 0.02 GeV, increasing m_c shifts y distribution to lower y, reducing the light quark mass moves it further forward

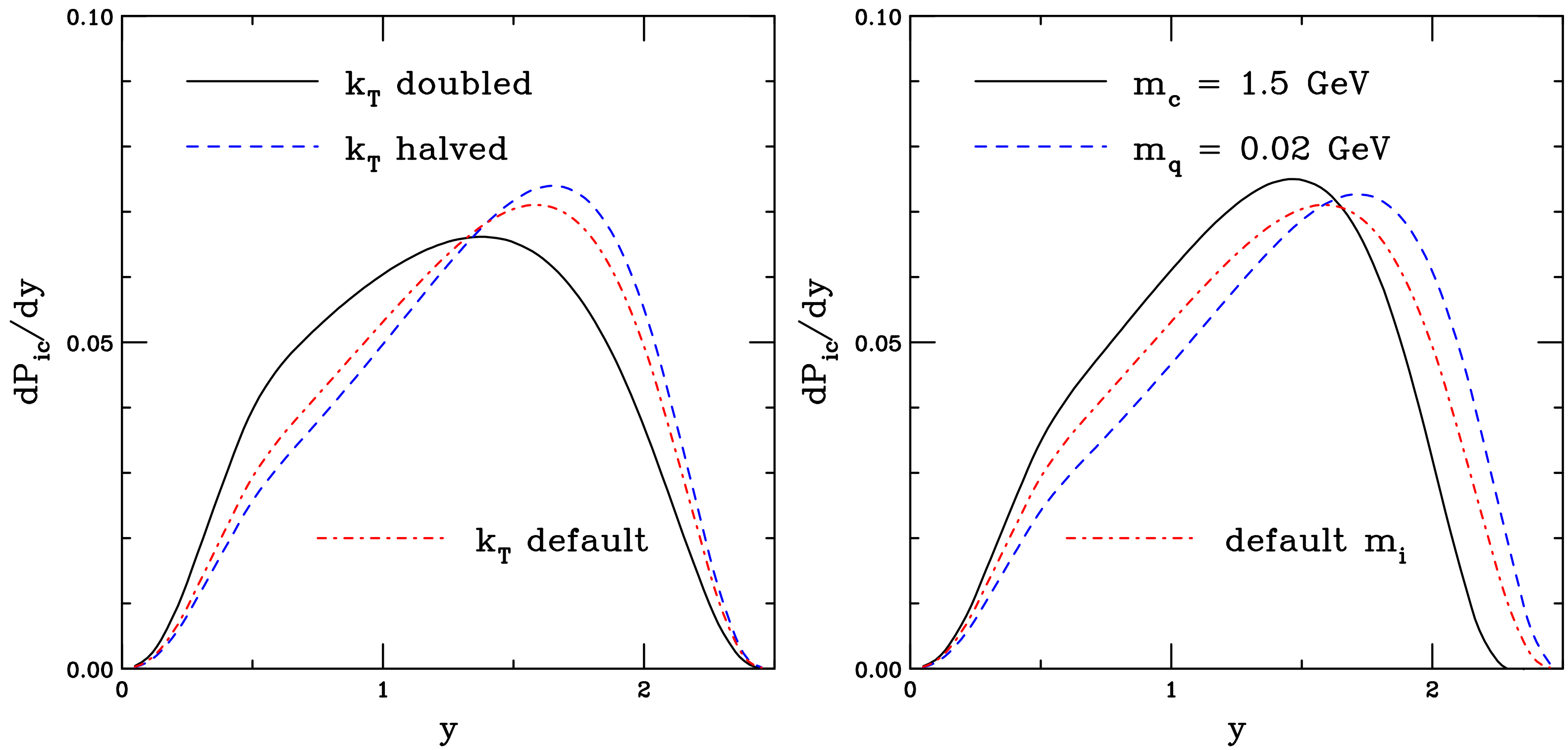

Figure 9: The probability distributions for J/ψ production from a five-particle proton Fock state as a function of y for $\sqrt{s_{NN}} = 15.4$ GeV. The dot-dashed red curve employs the default values, $k_q^{\max} = 0.2$ GeV and $k_c^{\max} = 1.0$ GeV in both plots. On the left-hand side, the black solid curve shown the results for $k_q^{\max}$ and $k_c^{\max}$ increased by a factor of two while the blue dashed curve employs half the values of $k_q^{\max}$ and $k_c^{\max}$. On the right-hand side. the solid black curve shows the result for increasing m_c to 1.5 GeV, the dashed blue curve shows the result for lowering m_q to 0.02 GeV.

y Dependence of IC p_T Distributions

All results for QCD plus intrinsic charm, assumes p_T is integrated over all rapidity

Here the p_T distributions are shown when the rapidity range is restricted to $0 < y < 1$, green curve shows integration over all y

The p_T distribution shifts to higher rapidity and total is decreased as $\sqrt{s_{NN}}$ increases, at higher energies and midrapidity, there is no contribution from intrinsic charm

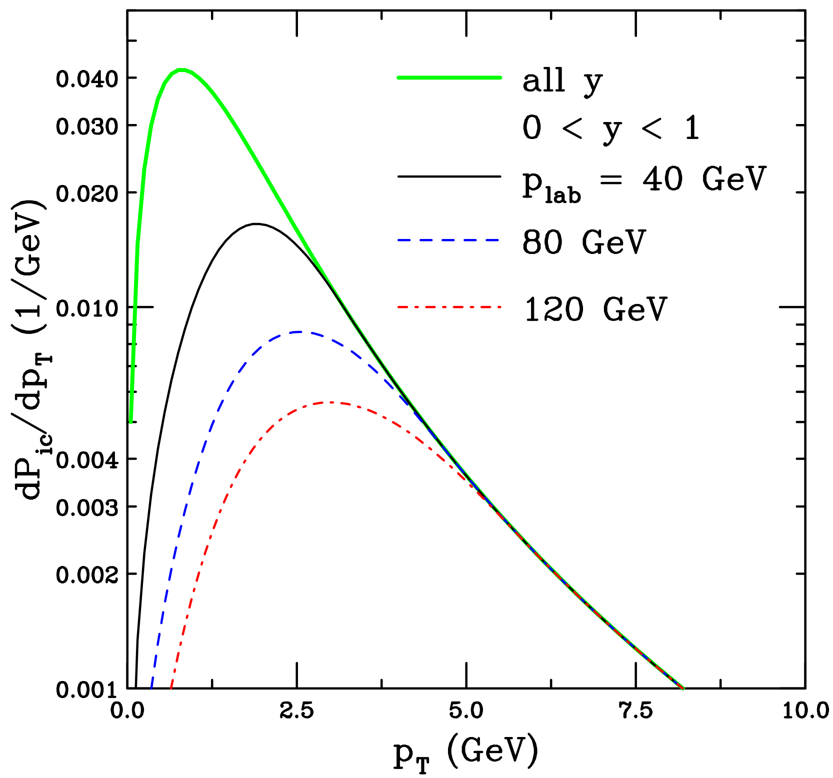

Figure 10: The probability distributions for J/ψ production from a five-particle proton Fock state as a function of p_T. The results are shown for all rapidity in the solid green curve. Results for restricting the rapidity range to $0 < y < 1$ are shown for $p_{\rm lab} = 40$, 80 and 120 GeV by the solid black, dashed blue and dot-dashed red respectively.

SeaQuest Predictions for $p + \mathrm{W}$ vs. x_F

The SeaQuest energy is the same as the upper NA60+ energy of 120 GeV but its acceptance is at forward x_F, not at midrapidity

The large x_F contribution from intrinsic charm changes the x_F dependence from effectively flat to decreasing with x_F

The EPPS16 uncertainties are shown on the pQCD contributions, the IC contributions are $P^0_{\mathrm{ic}\,5} = 0.1\%$, 0.31% and 1% from top to bottom on the middle and right plots, the right plot also includes absorption

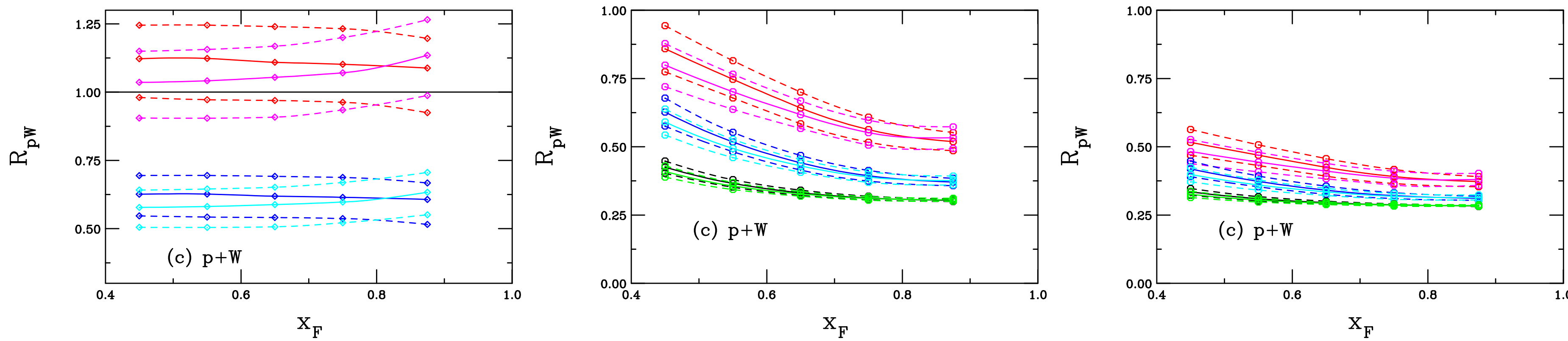

Figure 11: The nuclear modification factors for J/ψ production in SeaQuest as a function of x_F for the combined pQCD and intrinsic charm cross section ratios for tungsten targets relative to deuterium. There is no intrinsic charm in the left-hand plot; intrinsic charm with no nuclear absorption in the center plot; and intrinsic charm plus pQCD absorption in the right-hand plot. Results with EPPS16 and the same k_T in $p + \mathrm{d}$ and $p + A$ are shown in the red, blue and black curves while EPPS16 with an enhanced k_T kick in the nucleus are shown in the magenta, cyan and green curves. The probability for IC production is 0.1% in the red and magenta curves; 0.31% in the blue and cyan curves; and 1% in the black and green curves. The solid lines shown the results with the central EPPS16 set while the dashed curves denote the limits of adding the EPPS16 uncertainties in quadrature.

SeaQuest Predictions for $p + \mathrm{W}$ vs. p_T

Intrinsic charm dominantes the SeaQuest acceptance region and significantly reduces the effects of k_T broadening

The EPPS16 uncertainties are shown on the pQCD contributions, the IC contributions are $P^0_{\mathrm{ic}\,5} = 0.1\%$, 0.31% and 1% from top to bottom on the middle and right plots, the right plot also includes absorption

Absorption aids the intrinsic charm dominance but may be overestimated, the value of 9 mb was taken for $x_F \sim 0$ so it could be lower in the forward region

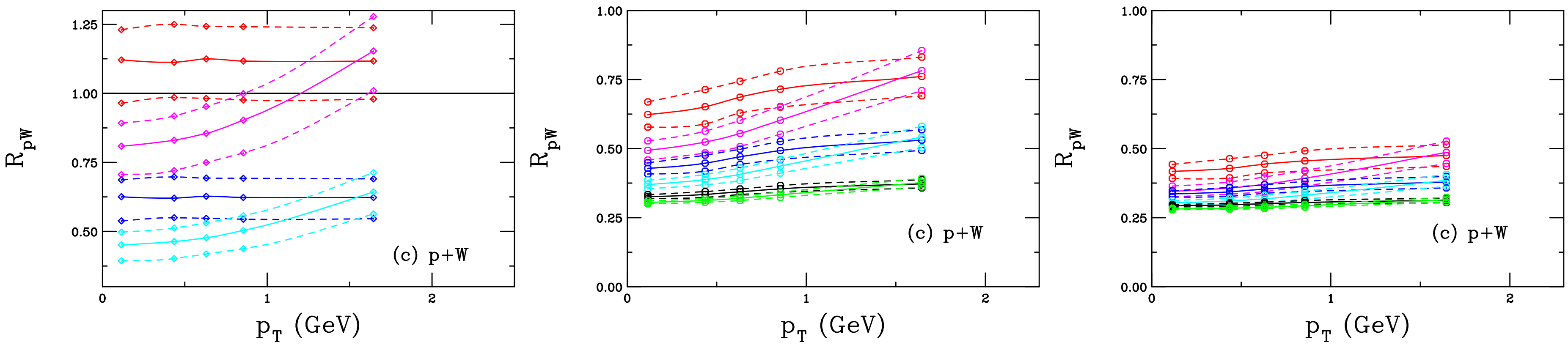

Figure 12: The nuclear modification factors for J/ψ production in SeaQuest as a function of p_T for the combined pQCD and intrinsic charm cross section ratios for tungsten targets relative to deuterium. There is no intrinsic charm in the left-hand plot; intrinsic charm with no nuclear absorption in the center plot; and intrinsic charm plus pQCD absorption in the right-hand plot. Results with EPPS16 and the same k_T in $p+\mathrm{d}$ and $p+A$ are shown in the red, blue and black curves while EPPS16 with an enhanced k_T kick in the nucleus are shown in the magenta, cyan and green curves. The probability for IC production is 0.1% in the red and magenta curves; 0.31% in the blue and cyan curves; and 1% in the black and green curves. The solid lines shown the results with the central EPPS16 set while the dashed curves denote the limits of adding the EPPS16 uncertainties in quadrature.

Comparison with α Extracted from E866 J/ψ Data

Update on previous calculations (PRC 61, 035203 (2000)), now with p_T ratios

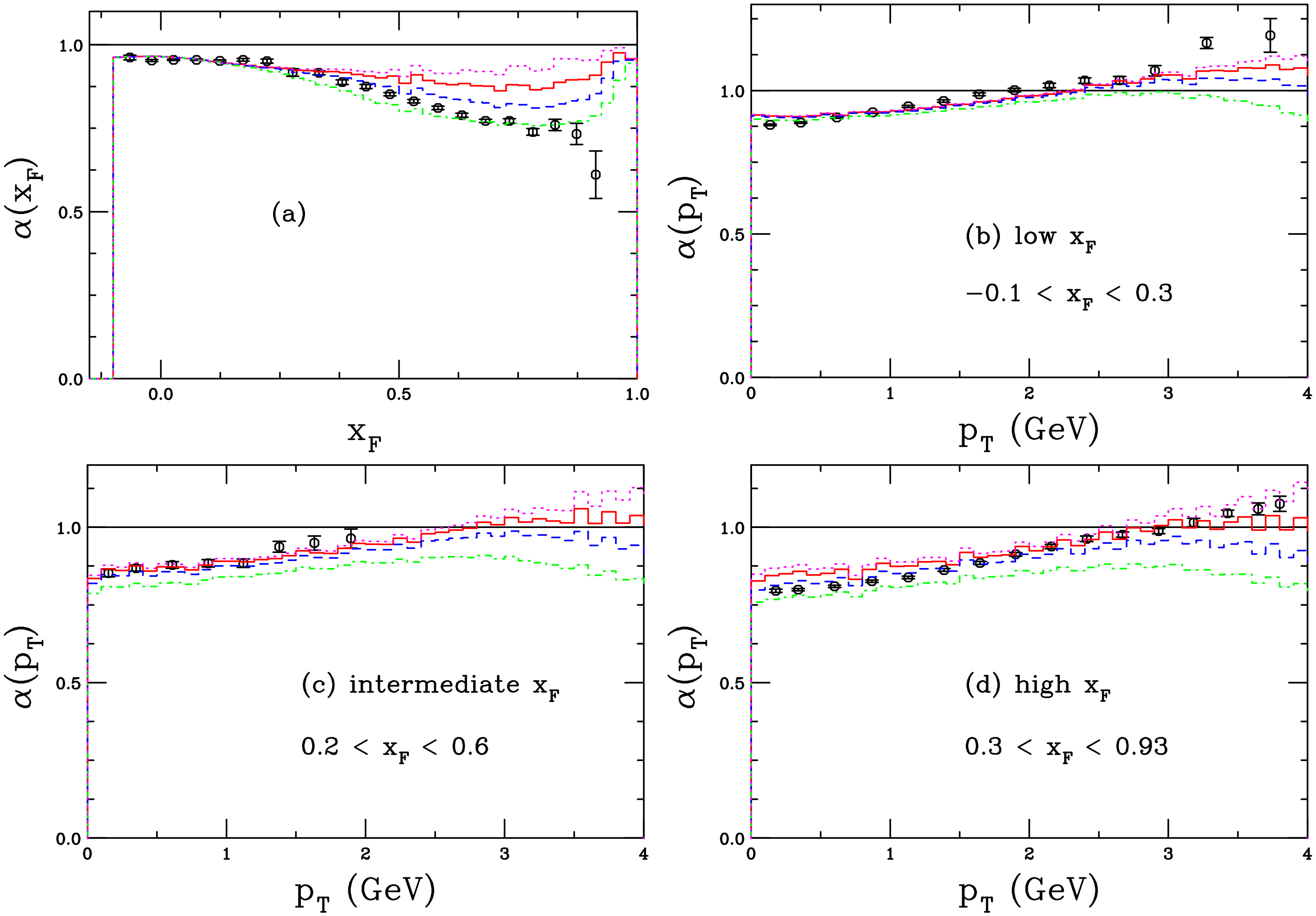

Figure 13: The exponent $\alpha(x_F)$ (a) and $\alpha(p_T)$ for low x_F (b), intermediate x_F (c), and high x_F (d). The dotted magenda curves use $P^0_{\rm ic\,5} = 0$ while the solid red, dashed blue, and dot-dashed green curves show $P^0_{\rm ic\,5} = 0.1\%$, 0.31% and 1% respectively. The E866 data (PRL **84**, 3256 (2000)) are the black points. From: RV, PRC **103**, 035204 (2021).

E866 J/ψ x_F and p_T Distributions

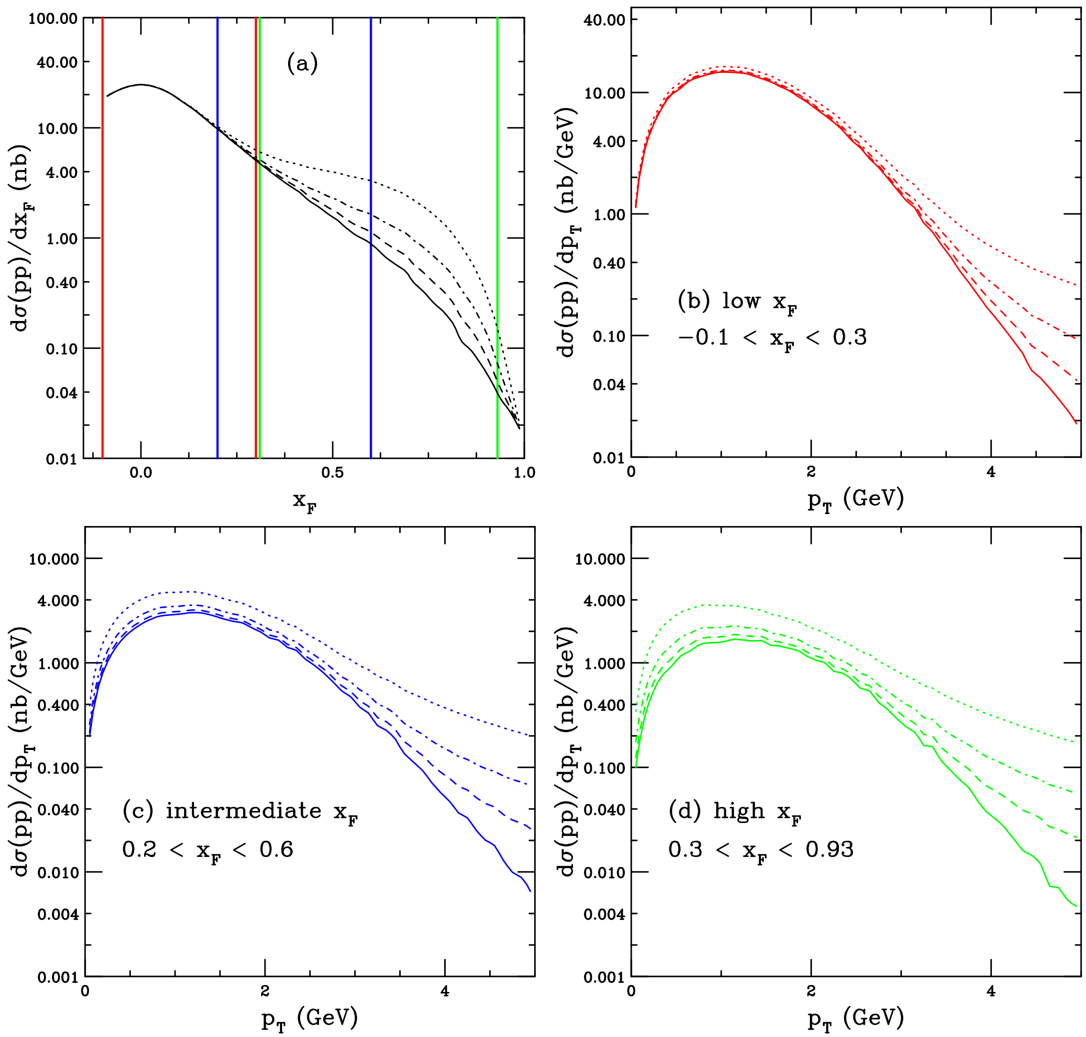

Figure 14: The J/ψ cross sections in $p+p$ collisions at $\sqrt{s} = 38.8$ GeV with and without IC as a function of x_F (a) and p_T at low (b), intermediate (c), and high x_F (d). The solid curves do not include IC while the dashed, dot-dashed and dotted curves use $P^0_{\rm ic\,5} = 0.1\%$, 0.31% and 1% respectively. The colored vertical bars on the x_F distributions show the x_F limits of the p_T distributions in (b)-(d) and matches the color of the curves in (b)-(d). RV, PRC **103**, 035204 (2021).

Rapidity and p_T $p+\mathrm{Pb}$ Ratios: No Intrinsic Charm

Upper curves do not include absorption, lower curves employ $\sigma_{\rm abs} = 9$, 10 and 11 mb for $p_{\rm lab} = 120$, 80 and 40 GeV respectively

Rapidity distributions do not depend on k_T kick, only absorption, increasing beam energy broadens rapidity distribution, increasing absorption gives lower $R_{p\rm Pb}$

p_T distributions without k_T kick flat, higher incident energy goes further into anti-shadowing region, increasing energy also increases size of k_T kick

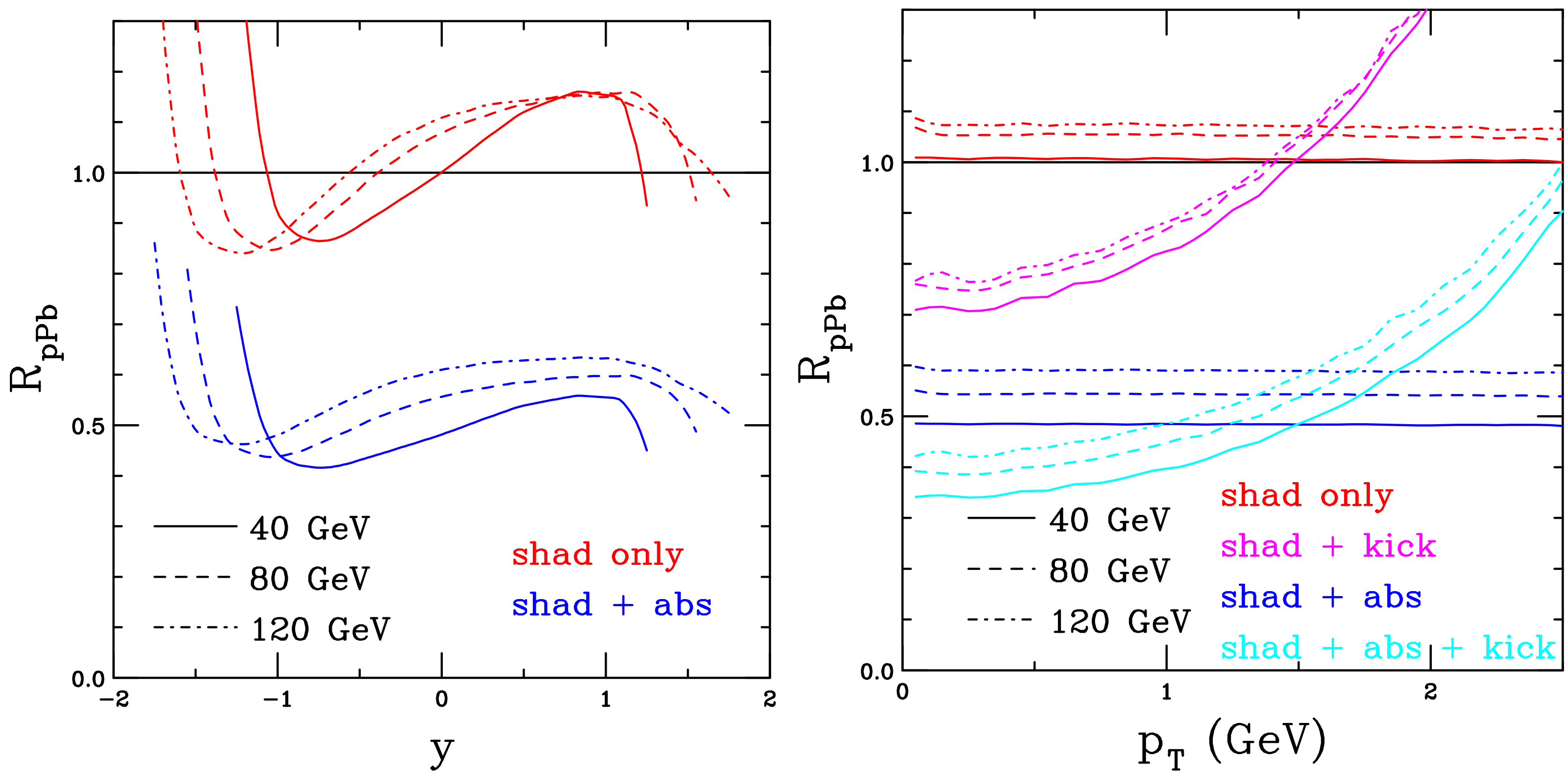

Figure 15: The nuclear modification factors for J/ψ production as a function of y (left) and p_T (right) for pQCD production alone for lead targets relative to proton. The solid, dashed and dot-dashed curves are for $p_{\rm lab} = 40$, 80 and 120 GeV respectively. The curves are for nPDF effects alone (red), nPDFs with an additional k_T kick (magenta), nPDFs and absorption (blue), and nPDFs, absorption and k_T broadening (cyan). Note that the rapidity distributions do not depend on the k_T broadening.

$R_{p\mathrm{Pb}}$ as a function of y: With Intrinsic Charm

Upper curves do not include absorption, lower curves employ $\sigma_{\mathrm{abs}} = 9$, 10 and 11 mb for $p_{\mathrm{lab}} = 120$, 80 and 40 GeV respectively

At these energies, $R_{p\mathrm{Pb}}$ is overwhelmed by intrinsic charm, even at midrapidity with $P^0_{\mathrm{ic}\,5} = 0.1\%$, unlike higher energy E866 results

At low center of mass energies, the rapidity distribution is not boosted very much. The energy dependence is quite strong.

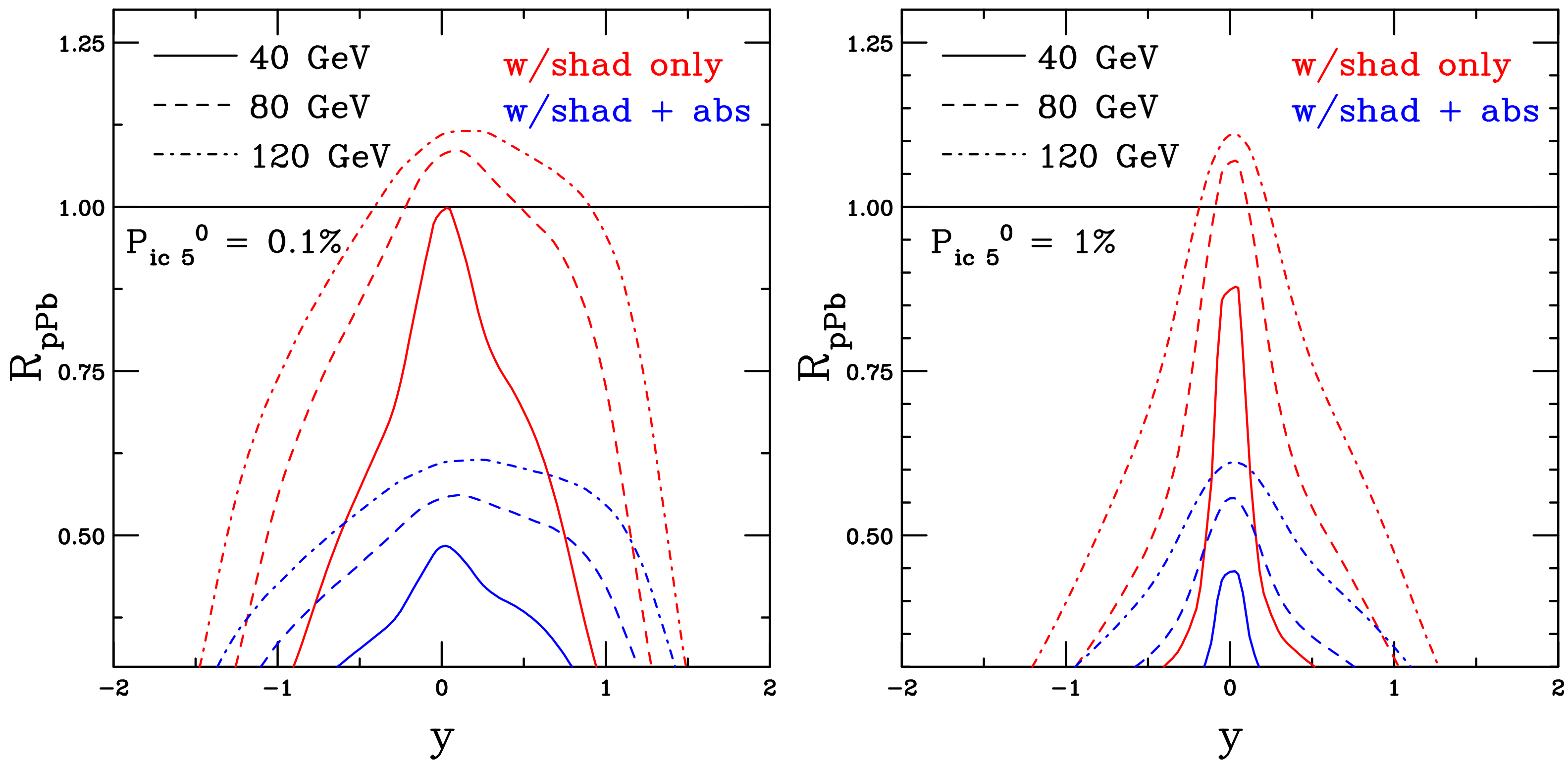

Figure 16: The nuclear modification factors for J/ψ production as a function of y for lead targets relative to proton with $P^0_{\mathrm{ic}\,5} = 0.1\%$ (left) and 1% (right). The solid, dashed and dot-dashed curves are for $p_{\mathrm{lab}} = 40$, 80 and 120 GeV respectively. The red curves are for nPDF effects alone on the pQCD contribution while the blue dashed curves include absorption on the pQCD component. Note that the rapidity distributions do not depend on the k_T broadening.

$R_{p\mathrm{Pb}}$ as a function of p_T: With Intrinsic Charm

Upper curves do not include absorption, lower curves employ $\sigma_{\mathrm{abs}} = 9$, 10 and 11 mb for $p_{\mathrm{lab}} = 120$, 80 and 40 GeV respectively

The intrinsic charm contribution is integrated over all rapidity, if it was restricted to midrapidity, $0 < y < 1$ for example, the p_T dependence would be reduced, only contributing at higher p_T

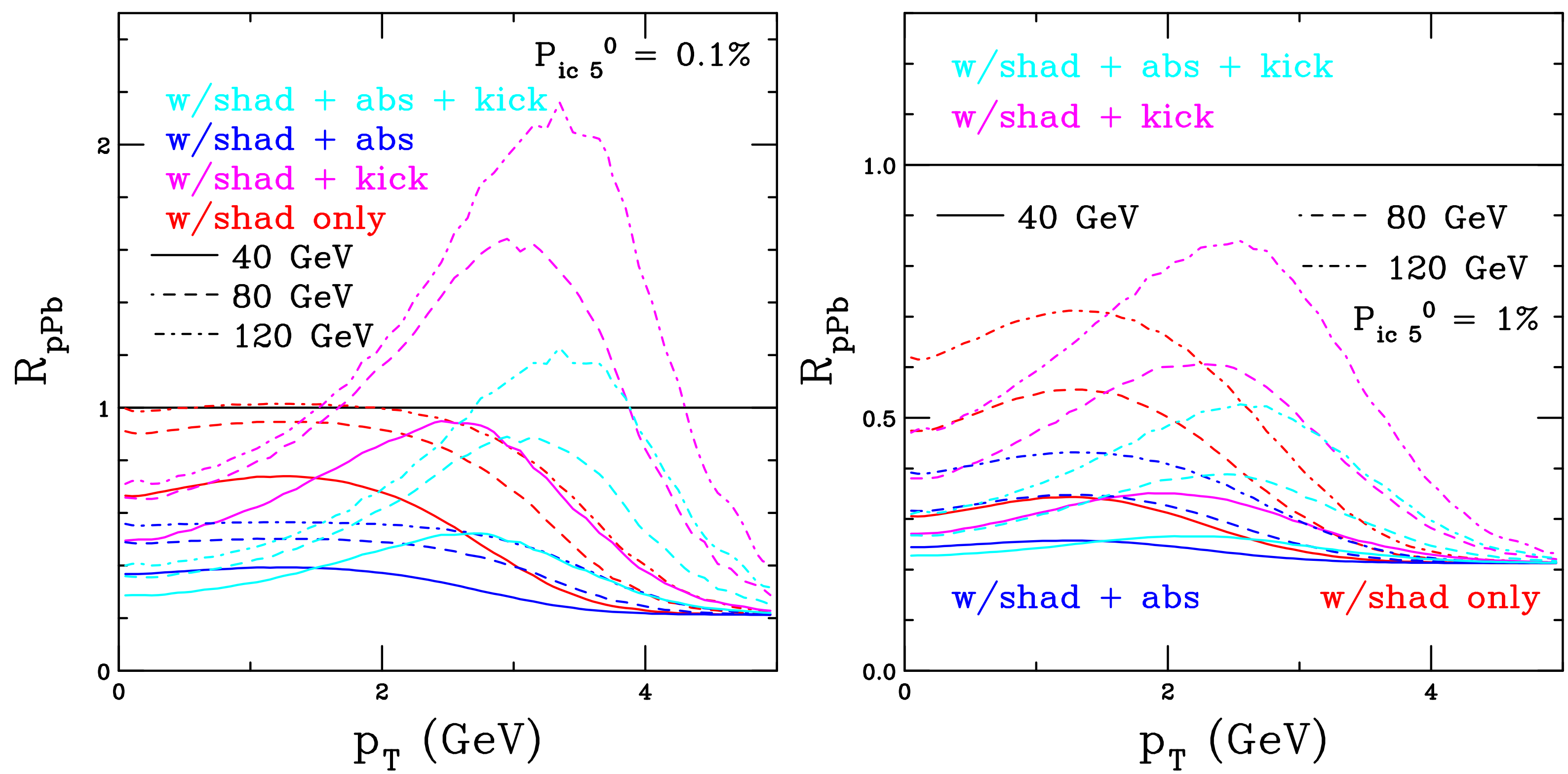

Figure 17: The nuclear modification factors for J/ψ production as a function of p_T for lead targets relative to proton with $P^0_{\mathrm{ic}\,5} = 0.1\%$ (left) and 1% (right). The solid, dashed and dot-dashed curves are for $p_{\mathrm{lab}} = 40$, 80 and 120 GeV respectively. The curves are for nPDF effects alone (red), nPDFs with an additional k_T kick (magenta), nPDFs and absorption (blue), and nPDFs, absorption and k_T broadening (cyan).

$p + p$ distributions as a function of y and p_T: With and Without Intrinsic Charm

All p_T calculations assume integration over all y, the intrinsic charm contribution would be overestimated if the contribution would be restricted to midrapidity – this effect becomes larger at higher energies, there would be no contribution to the midrapidity p_T distribution at all at RHIC and LHC energies

The strong energy dependence of the intrinsic charm contribution is evident; any pQCD nuclear effects would be quickly overwhelmed

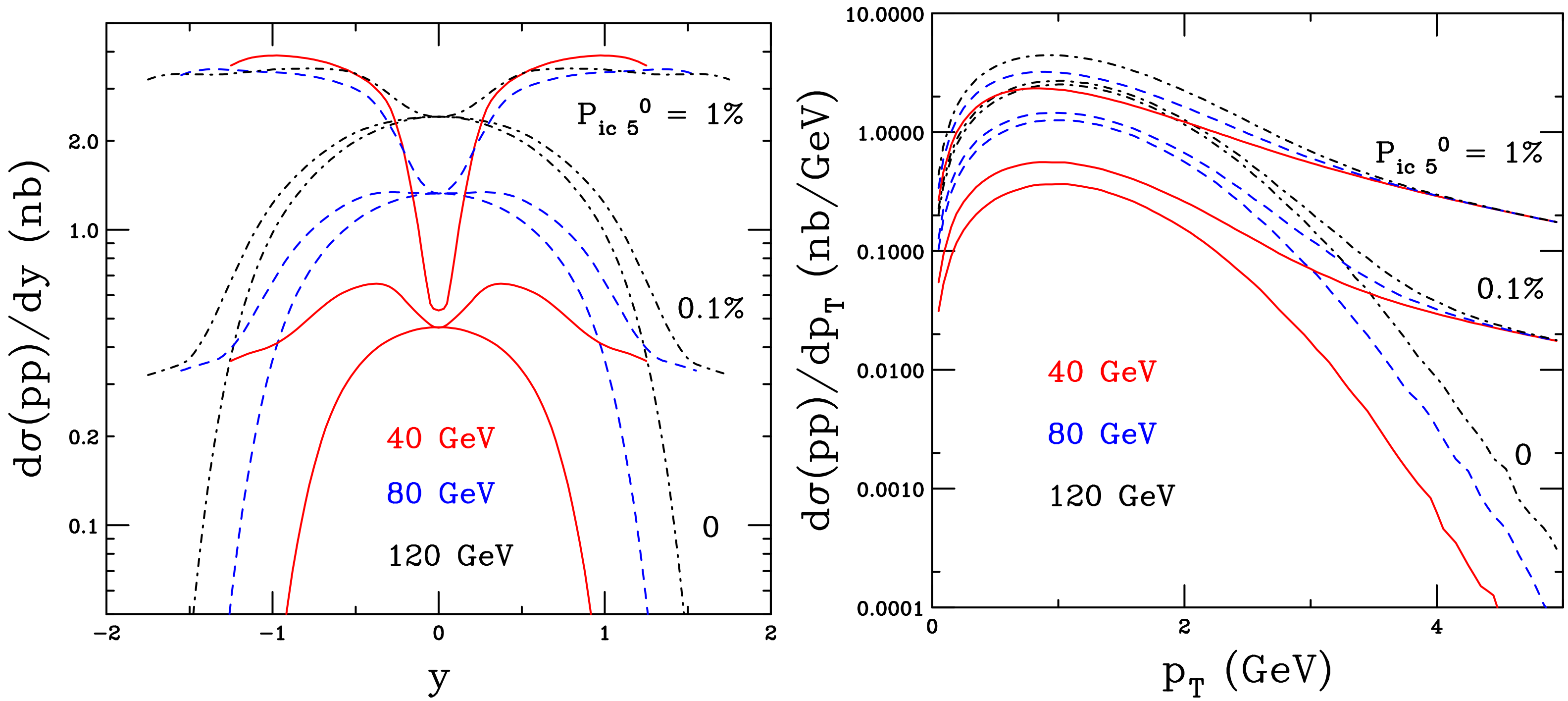

Figure 18: The nuclear modification factors for J/ψ production as a function of y (left) and p_T (right) in $p+p$ collisions with $P^0_{\mathrm{ic}\,5} = 0\%$ (bottom curves) 0.1% (middle curves) and 1% (upper curves). The solid red, blue dashed and black dot-dashed curves are for $p_{\mathrm{lab}} = 40$, 80 and 120 GeV respectively.

Summary

The low center of mass energies of NA60+ could provide stringent constraints on the energy dependence of intrinsic charm in the hadron wavefunction

Together with the SeaQuest J/ψ data at similar energies but more forward coverage, combined with an analysis of the perturbative and intrinsic charm contributions, could determine the probability of J/ψ production from intrinsic charm

The same formalism is being applied to J/ψ and D^0 production with the fixed-target SMOG device for LHCb, stay tuned